JOURNAL OF AIRCRAFT
Vol. 37, No. 2, March–April 2000

Nonlinear Design Loads for Maneuvering Elastic Aircraft

D. E. Raveh* and M. Karpel†
Technion—Israel Institute of Technology, 32000 Haifa, Israel
and
S. Yaniv‡
Israel Military Industries, Ltd., 47100 Ramat-Hasharon, Israel

A computationally efficient scheme for maneuver load analysis, based on nonlinear aerodynamics, is presented. The kernel of the scheme is a computational fluid dynamics (CFD) code for solving the Euler/Navier–Stokes equations for a fixed-shape configuration. A modal structural model is used for elastic-shape updates, and a trim corrections algorithm is used for varying the incidences and control surface deflections until the user-defined maneuver is attained. Computational efficiency is obtained by performing a few elastic-shape changes and maneuver trim updates, all within the fluid dynamics analysis, during the steady-state flowfield convergence. The modal approach, where the structure is represented by a set of its low-frequency vibration modes, greatly simplifies the CFD–structure interface, minimizes the amount of structural data required, and allows simple shape updates of the aerodynamic grid. It is shown that the total computation time required for flowfield convergence for a maneuvering elastic aircraft is typically almost identical to that of the rigid aircraft with given trim variables. The method is demonstrated with a realistic wing–fuselage–elevator transport aircraft model performing symmetric maneuvers at Mach 0.85.

Introduction

STATIC aeroelastic effects on aircraft performance and design loads are traditionally calculated using linear aerodynamic models. Methods for calculating the linear aerodynamic force coefficients, such as the doublet-lattice method (DLM),[1] are well established and integrated into commercial softwares for structural–aeroelastic analysis and design optimization, such as MSC/NASTRAN[2] and ASTROS.[3] However, these linear models often might be inadequate when used for flight vehicles cruising and maneuvering in the transonic-speed range, where embedded shock waves affect the flowfield significantly. For this reason, the static branch of computational aeroelasticity has evolved, integrating computational fluid dynamics (CFD) schemes with various types of structural models. Static computational aeroelasticity works described in the literature differ in the CFD scheme used, in the structural model, in the way the two disciplines are brought together, and in the amount of generality and complexity of the studied test cases.

The early works that combined CFD with elasticity used simple structural models and were demonstrated on an elastic wing.[4–6] Tatum and Giles[7] addressed a complete aircraft configuration. Using a full potential aerodynamic method (SIMP), together with an equivalent plate structural model, they implemented an iterative solution procedure for obtaining aerodynamic loads and structural deflections for the free-flying aircraft at user-specified flight conditions. The model selected by Tatum and Giles was that of a fighter aircraft consisting of only one aerodynamic grid segment. This choice of model was made to meet the requirements of the CFD code used by the authors that allowed only single-body analysis. Consequently, the aircraft was trimmed only by vectoring the thrust of the engine, and the common combination of varying the angle of attack and the control surfaces angles for achieving trim was not studied. Vinh et al.[8] added a trim routine to the CAP-TSD code.[9] Their work suggests a feedback algorithm to obtain vehicle trim during steady-state flowfield convergence. Because the code used is time accurate, stability and control derivatives also could have been estimated from the transient response. Schuster et al.[10] addressed the problem of computing the flowfield about flexible fighter aircraft operating at extreme flight conditions, such as high angles of attack and high transonic Mach numbers. Because these flows involve strong shock waves and detached boundary layers, for which the small disturbance assumption is no longer valid, Schuster et al. based their work on the Lockheed Euler/Navier–Stokes aerodynamic method (ENS3D) combined with an influence-coefficient structural model. In a later work Schuster[11] demonstrated the use of this aeroelastic analysis method for improving the performance of fighter wings through simultaneous application of control surface deflection and aeroelastic twist. Guruswamy[12] performed aeroelastic computations on a wing–fuselage configuration using an Euler/Navier–Stokes aerodynamic method (ENSAERO) coupled with a finite element beam-type structural model. In a later work, Obayashi and Guruswamy[13] suggested solving the dynamic equations of the structure, instead of the static equations, with added artificial damping, to achieve a smooth structural response and, therefore, prevent instabilities in the fluid dynamics computations.

This paper describes the development of an efficient computational scheme for defining the aerodynamic loads on maneuvering flexible flight vehicles, with several trim variables, based on an Euler solver. It is intended for evaluation of structural design loads at flight conditions for which the aerodynamic nonlinearity is important but not extremely strong. The modal aeroelastic approach of Refs. 14 and 15, which showed excellent efficiency and accuracy with linear aerodynamics, is used to evaluate the elastic deformations and to trim the free aircraft. A computationally efficient scheme is obtained by applying a relatively small number of shape and trim updates to achieve static equilibrium, during flowfield convergence. A similar approach was used by Karpel et al.[16] for flexible rockets in supersonic flight with one trim variable. The scheme is expanded here to deal in a practical way with realistic aircraft whose trimmed condition is achieved through the use of varied incidences, control-surface deflections, and rotation rates.

Aeroelastic Method

An Euler/Navier–Stokes code of Yaniv[17] is used for the fluid dynamics computations. The flow, in general, is assumed to be compressible, viscous, and turbulent. In the current study, however, the viscosity effects are neglected and the Euler equations are used.

Received 19 May 1998; revision received 15 April 1999; accepted for publication 15 October 1999.

*Graduate Student, Aerospace Faculty; currently Postdoctoral Fellow, School of Aerospace Engineering, Georgia Institute of Technology, Atlanta, GA 30332-0150. Member AIAA.

†Professor, Faculty of Aerospace Engineering. Senior Member AIAA.

‡Team Leader, Computational Fluid Dynamics.

This reduces the required computational resources significantly. A semidiscrete finite volume method using central differencing in space with explicit multistage time-stepping scheme is employed. A steady-state solution to the time-dependent Euler equations is obtained by iterating in time using local time steps and implicit residual smoothing.

The maneuver analysis is made on three levels of iterative processes. The innermost level contains the CFD analysis for a fixed-shape configuration that, if iterated until convergence, provides the aerodynamic load distribution on the rigid aircraft. The next iterative level introduces the structural elasticity that is combined with the aerodynamic loading to obtain the corresponding deformed shape. This level, if iterated until convergence, provides a load distribution that agrees with the shape distribution of the elastic aircraft. The outermost level contains the maneuver trim loop at which the incidences and control surface deflection angles are varied to obtain the total aerodynamic forces and moments implied by the user-defined maneuver.

For computational efficiency, both the elastic deformations and trim corrections are introduced during the CFD solution convergence. The user defines a number of CFD iterations, after which elastic deformations are computed and applied to the CFD grid, and a number of elastic deformations, after which maneuver corrections are made. Typically, the number of CFD iterations between two successive elastic deformation updates is 5–10% of the number of iterations required for flowfield convergence. The shape and trim parameters are not updated after each CFD iteration to avoid excessive computations and also to avoid numerical instabilities in the flow computations.

A coupled aerodynamic–structural scheme requires special methods for interfacing the CFD and structural models, calculating the elastic deformations, moving the body-fitted aerodynamic grid as the elastic aircraft deflects, and trimming to achieve the required aerodynamic coefficients.

CFD–Structure Interface

Generally, the CFD–structure interface refers to the transformation to the structural grid of aerodynamic forces that are computed on the aerodynamic grid, and to the mapping of the elastic deflections computed on the structural finite element nodes to the aerodynamic grid. When the modal structural approach is taken, with the structure represented by a set of its low-frequency vibration modes, the CFD–structure interfacing task reduces to mapping the modes to the aerodynamic surface grid points. After this is done, the computation of elastic deformations can be carried on within the fluid dynamics computations.

An interface difficulty arises from the different nature of the discretizations of the two disciplines. Whereas the grid points of the aerodynamic model are distributed on the external surface and outside of it, the nodes of the structural model are placed on, and inside, the surface. Typically, the aerodynamic grid is very dense, and its grid points are uniformly distributed. The structural model, on the other hand, has nodes located on the elements carrying the loads and, therefore, are not uniformly distributed. The structural grid is usually coarser than the CFD surface grid.

The physical aero-structure interface points lie on general surfaces in three-dimensional space. Therefore a three-dimensional interpolation method is required. With a surface segment defined by $il \times jl$ aerodynamic grid points, the displacement of point (i, j) is

$$\bar{w}(i, j) = \bar{f}[\xi(i, j), \eta(i, j), \zeta(i, j)] \qquad i = 1, \ldots, il, \quad j = 1, \ldots, jl \tag{1}$$

where $\bar{f}$ is the spline displacement function and ξ, η, and ζ are the coordinates of the surface points. To overcome the difficulties in the application of the three-dimensional interface method, some constraining rules are applied to the shape changes, for interfacing purposes only. The aircraft is divided into two geometrical entities: lifting surfaces and slender bodies. Each lifting surface can be represented by one or more reference planes, where the structural deformations are limited to directions perpendicular to these planes, based on a two-dimensional spline scheme, such that

$$\bar{w}(i, j) = \bar{f}[\xi(i, j), \eta(i, j)] \qquad i = 1, \ldots, il, \quad j = 1, \ldots, jl \tag{2}$$

The infinite plate spline method by Harder and Desmarais[18] is applied to each reference plane separately. The new shape of the spline surface is defined such that it passes through the known structural displacements at given structural coordinates. The displacement of each aerodynamic point is set according to the point location on the deformed spline surface. For the interface between structural and aerodynamic points along a slender body, such as the fuselage, a beam spline was used[2] that follows the same logic of the surface spline. To maintain continuity between the fuselage and the lifting surfaces, as well as between the subsurfaces, a tree structure is used. The fuselage serves as the trunk, and the components coming out of it serve as the branches. The deformation of branch points is determined by the branch spline, plus a correcting displacement that maintains the branch interface to the trunk. Each branch can serve as a trunk to lower hierarchy branches.

Figure 1 shows the first wing-bending mode and first wing-torsion mode of the model aircraft, mapped onto the aerodynamic surface grid points. Figure 1 also shows part of the elevator mode. This is an artificial mode that describes unit rigid elevator rotation, which is used as a trim variable in symmetric maneuvers. The depicted mode is used for the aerodynamic grid update that follows elevator deflections. It can be seen that there is a blending zone in the elevator mode near the elevator root. This is done to avoid discontinuities in the updated aerodynamic grid.

Structural Elastic Deflections

The static elastic equation in generalized coordinates is solved within the fluid dynamics computations according to

$$[K_E]\{\xi_E\} = \{F_E\} \tag{3}$$

where $[K_E]$ is the generalized stiffness matrix associated with a low-frequency set of the free–free elastic vibration modes, and $\{F_E\}$ is the

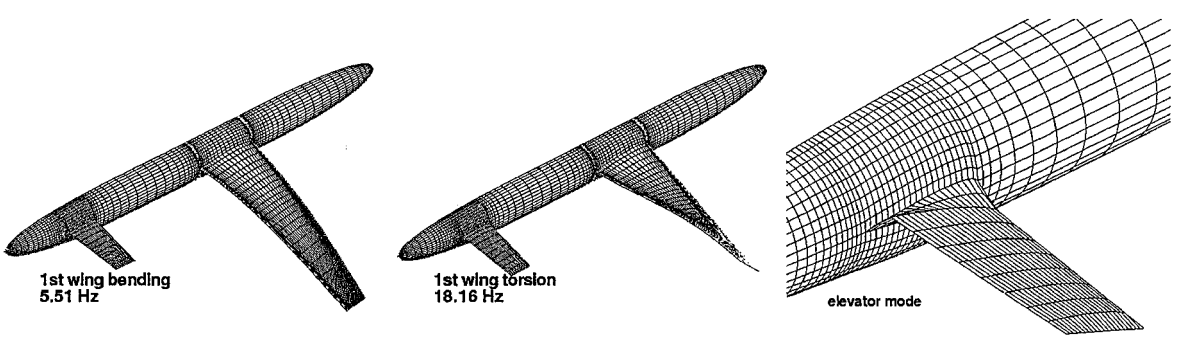

Fig. 1 Deformed aerodynamic surface grids.

associated generalized aerodynamic force vector. The generalized forces are obtained from summing the aerodynamic forces at the aerodynamic surface grid points according to

$$\{F_E\} = [\phi_E]^T \{F\} \tag{4}$$

where $[\phi_E]$ is the modes matrix, splined to the aerodynamic surface grid points, and $\{F\}$ is the aerodynamic force vector at the aerodynamic surface grid points. Because the elastic modes are orthogonal to the rigid-body modes with respect to the structural mass matrix, inertia relief effects in the right-hand side of Eq. (3) are taken care of automatically.[14] The rigid-body counterpart of Eq. (3) is used subsequently in the maneuver trim process.

After the elastic equation is solved for a set of generalized coordinates $\{\xi_E\}$, the new deformed shape of the aerodynamic surfaces is obtained as a combination of the structural vibration modes, according to

$$\{u_E\} = [\phi_E]\{\xi_E\} \tag{5}$$

where $\{u_E\}$ is the elastic displacement vector at the aerodynamic surface grid points.

Using the modal approach, the modal stiffness matrix and the modes matrix are the only structural data required for the aeroelastic analysis. These matrices are calculated by the finite element code and are read by the computational aeroelastic scheme, only once, as it starts. Because the number of structural modes used is typically small (in this work 10 structural modes were found to be sufficient) very little structural data are required to be transferred.

Aerodynamic Grid Update

Once the aerodynamic surface grid points have been deflected to account for the structural deformation, the field grids must also be deflected accordingly. The deformed grid should satisfy a few basic requirements: grid lines of the same family should not intersect, the updated grid should remain fairly smooth, and the grid deformations should decay rapidly such that points near the deformed surface move with the surface, whereas points near the far field do not move.

The field grid is regenerated by redistributing points along ζ grid lines that are almost normal to the surface. Each grid point is displaced by a value equal to the surface displacements multiplied by its normalized arc length from the far field.

Maneuver Trim

Structural design loads are based on aerodynamic loads of prescribed aircraft steady maneuvers. When solving for a prescribed maneuver, the aerodynamic coefficients (the lift coefficient and the moment coefficient for the case of a symmetric maneuver) are defined by the maneuver, whereas the unknown trim variables are the incidences and control surfaces deflections that would provide the required aerodynamic coefficients. The symmetric aerodynamic coefficients should satisfy

$$qS \begin{Bmatrix} C_L \\ C_M \bar{c} \end{Bmatrix}_{\text{trim}} = [M]\{\ddot{\xi}\} \tag{6}$$

where C_L is the lift coefficient, C_M is the moment coefficient, $\bar{c}$ is the reference chord, and $\bar{q}$ is the dynamic pressure. Similar expressions can be written for antisymmetric or asymmetric maneuvers. The current values of the aerodynamic coefficients are calculated during the CFD solution by

$$qS \begin{Bmatrix} C_L \\ C_M \bar{c} \end{Bmatrix}_{\text{current}} = [\phi_R]^T \{F\} \tag{7}$$

where $[\phi_R]$ is the rigid-body modes matrix. The fluid dynamics computation starts with an initial estimate of the trim variables, which is updated, during the flowfield convergence, according to the differences between the desired and the current values of the aerodynamic coefficients. The equation for maneuver trim corrections, in a symmetric maneuver, is

$$\begin{Bmatrix} C_L \\ C_M \bar{c} \end{Bmatrix}_{\text{trim}} = \begin{Bmatrix} C_L \\ C_M \bar{c} \end{Bmatrix}_{\text{current}} + \begin{bmatrix} \tilde{C}_{L\alpha} & \tilde{C}_{L\delta} \\ \tilde{C}_{M\alpha} & \tilde{C}_{M\delta} \end{bmatrix} \begin{Bmatrix} \Delta\alpha \\ \Delta\delta \end{Bmatrix} \tag{8}$$

where α and δ are the current values of trim variables (angle-of-attack and elevator deflection), and $\Delta\delta$ and $\Delta\alpha$ are the maneuver corrections that drive the trim variable closer to the trim solution. $\tilde{C}_{L\alpha}$, $\tilde{C}_{M\alpha}$, $\tilde{C}_{L\delta}$, and $\tilde{C}_{M\delta}$ are the estimated derivatives of the aerodynamic coefficients with respect to the symmetric trim variables. With nonlinear CFD analysis, the dependencies of the aerodynamic coefficients on the trim variables are nonlinear and implicit. Therefore, numerical computation of the aerodynamic coefficients derivatives by finite difference is numerically expensive. To avoid the computation of the nonlinear derivatives, the trim corrections are computed based on approximated derivatives, such as the linear aerodynamic derivatives. This was practiced in this study, where the estimated linear sensitivities were obtained from an aeroelastic run using the aeroelastic module of MSC/NASTRAN. It was found that in cases where the coupling between the angle of attack and elevator is weak, that is, the angle of attack mainly controls the lift coefficient and the elevator deflection angle mainly controls the moment coefficient, the coupling terms $\tilde{C}_{M\alpha}$ and $\tilde{C}_{L\delta}$ can be neglected, still leading to a smooth convergence to the maneuver aerodynamic coefficients. In coupled configurations, however, equating the coupling terms to zero resulted in slow convergence, with undesirable oscillations of the values of the trim variables. However, the numerical example shows that the derivative estimates can be quite crude, still leading to the correct trim solution.

The variation of the angle of attack is introduced into the CFD as a change in the far-field conditions and is, therefore, easy to implement. The control surface deflections require a change in the configuration and regeneration of the aerodynamic grid. Regeneration of the aerodynamic grid is made in the same manner as in accounting for elastic deformations, using the elevator mode discussed earlier.

Angular rates associated with the maneuver are introduced to the aerodynamic analysis by adding terms to the fluid dynamics equations, to account for being written in a rotating system. This is an extension of the way rolling effects are considered by Yaniv.[17]

Numerical Example

Aircraft Model

A simple generic transport aircraft model that has all of the features necessary to verify the proposed methodology was created. The model aircraft includes a fuselage, wing, and all-movable tail. The wing and elevator are similar in shape and structure; both are tapered and swept aft. The cross-sectional profiles of the wing and elevator are scaled NACA 0012 symmetric profiles. The wing geometrical dimensions are aspect ratio 10, half-span 10 m, root chord 2.8 m, and leading-edge sweep angle 20 deg. The fuselage is 20 m long.

For the aerodynamic analysis, an H–C-type grid topology is used, H-type in the streamwise direction and C-type in the spanwise direction. Taking advantage of the multizone capability of the analysis code, the grid was divided into 24 zones, each describing a logical component such as wing upper/lower surface, fuselage, etc. Figure 2 describes i, k and j, k constant grid surfaces (only every other grid line is shown). The entire flowfield contains approximately 500,000 grid points.

Table 1 Weight summary, half-aircraft

Component	Weight, kg
Wing	1100
Elevator	405
Fuselage	2320
Fuel inside the fuselage	2000
Engine	700
Total weight	6525

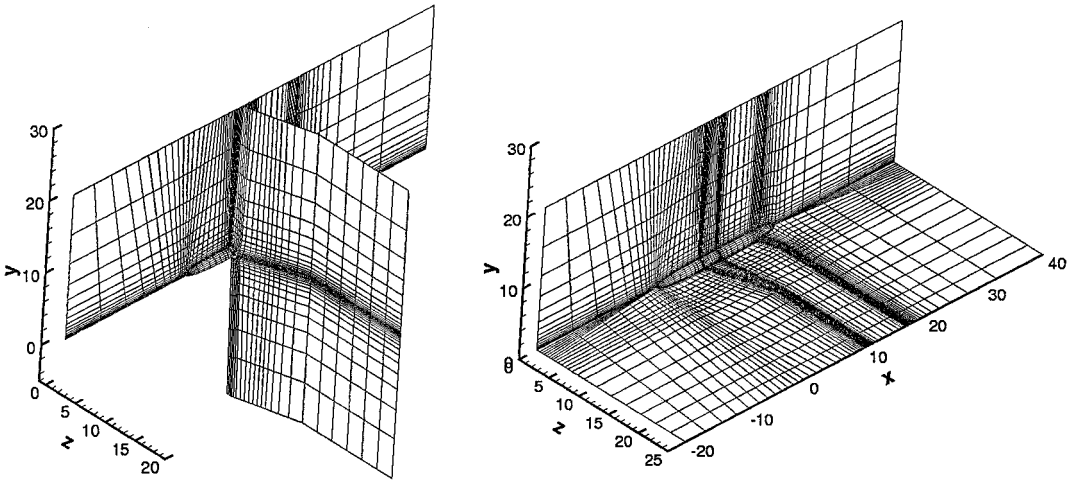

Fig. 2 Aerodynamic grid *i*, *k* and *j*, *k* constant surfaces.

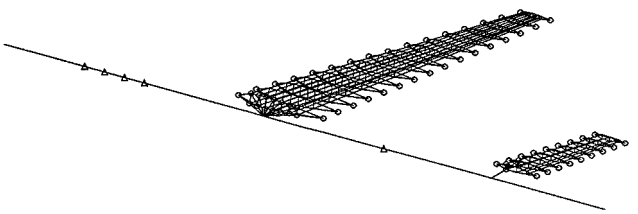

Fig. 3 Finite element model.

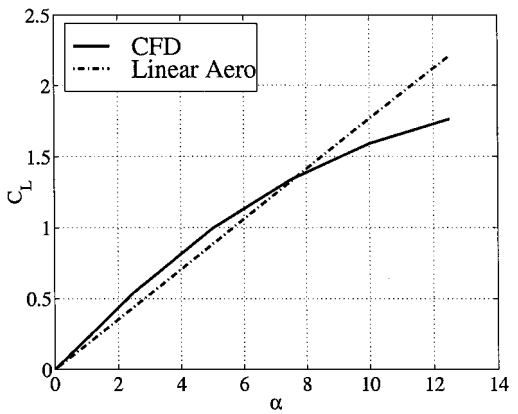

Fig. 4 Lift coefficient vs angle of attack.

The structure of the example aircraft was modeled in detail and analyzed using the finite element software MSC/NASTRAN. The wing and tail components were modeled by their torsion boxes, which include skin, ribs, spars, spar caps, and stringers. The fuselage component was modeled as a flexible bar. Figure 3 shows the finite elements model. A modal analysis was performed to provide the 10 low-frequency vibration modes and the corresponding generalized stiffness matrix required for the aeroelastic analysis. Table 1 summarizes the weights of the half-aircraft model.

Aeroelastic Analysis

The flowfield about the rigid-aircraft model was evaluated at Mach 0.85 and an altitude of 11,000 m, for various angles of attack. The resulting lift coefficient variation with the angle of attack is compared in Fig. 4 to the linear slope obtained from the aeroelastic module of MSC/NASTRAN using the DLM. Based on this dependency, an elastic analysis was performed at an angle of attack of 5 deg, which is typical of maneuver analyses of transports (corresponds to an approximately 3-*g* pullup maneuver) and at which the flowfield is not extremely nonlinear. The algorithm for elastic corrections was added to the fluid dynamics computation, updating the

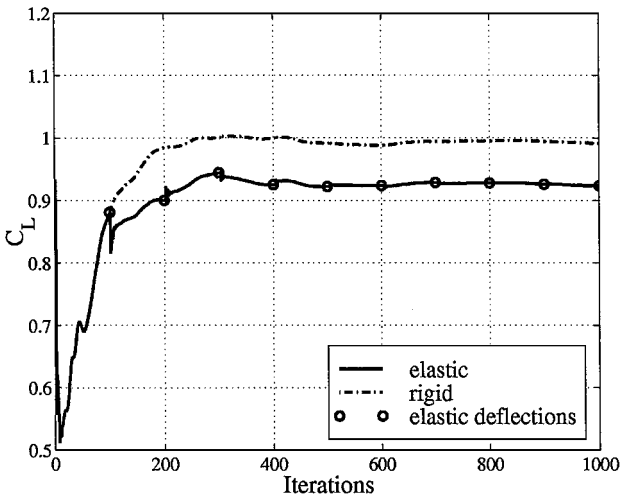

Fig. 5 C_L convergence history.

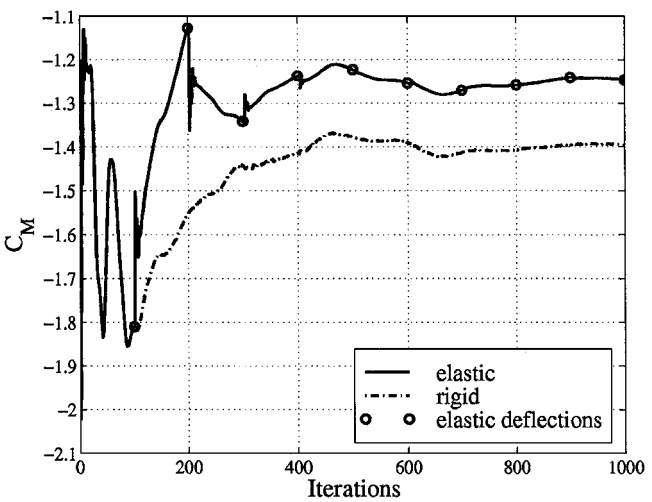

Fig. 6 C_M convergence history.

shape every 100 iterations. Figures 5 and 6 show the convergence history of the aerodynamic coefficients C_L and C_M, comparing the elastic- and rigid-run cases. The elastic lift coefficient converged to a value of 0.93, which is 6% less then the rigid lift coefficient. The elastic moment coefficient (calculated around the aircraft center of gravity with reference length of 1 m) was found to be 11% less than the rigid value. Examining the elastic wing deflections (shown in Fig. 7), it was found that the wing tip leading edge deflected by

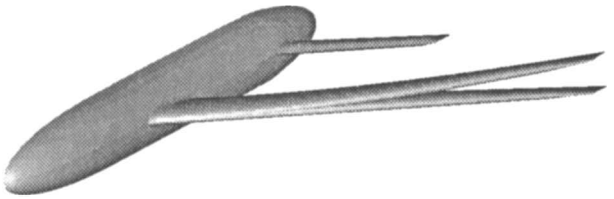

Fig. 7 Elastic deformations.

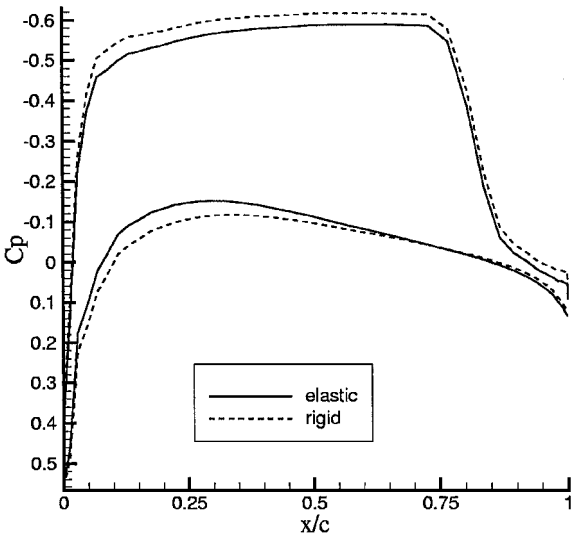

Fig. 8 Wing pressure distribution: rigid vs elastic.

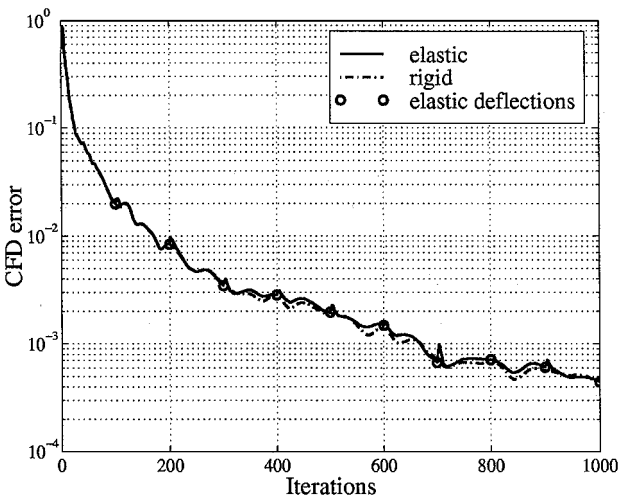

Fig. 9 Residual decay history.

0.21 m above the root and that the wing tip experienced a wash-out of 1.5 deg. Figure 8 shows the pressure coefficient along a wing section at 82% of the span for the elastic and rigid configurations. Both the tip wash-out and the section pressure agree with the reduction of the aerodynamic coefficients.

For comparison, a static aeroelastic run was conducted with the model aircraft, at the same flight conditions, using MSC/NASTRAN aeroelastic option with the doublet-lattice linear aerodynamic method. Contrary to the CFD predictions, the aircraft wing experienced a wash-in tip, leading to an increase of 6% in the lift coefficient ($C_{L\,\text{rigid}} = 0.83$, $C_{L\,\text{elast}} = 0.88$). This might indicate that the conventional design-loads methodology that adds elastic corrections based on linear aerodynamics to a rigid database might be misleading.

Figure 9 shows the history of residual decay of the elastic-run case compared to that of the rigid-run case. It is seen that the disturbances to the flowfield caused by the shape update have little effect on the residual and that the total number of iterations required for flowfield convergence is almost the same for the elastic- and rigid-run cases. The extra CPU time required for the grid update following every elastic deformation is only 0.7 s, compared to 60 s required for each CFD iteration. Therefore, because only few elastic deflections are made, the total extra CPU time required for the inclusion of aeroelastic effects in a typical flow computation is negligible.

Next, the algorithm for trim corrections was added, and the aircraft was required to perform a 4-g pullup maneuver (corresponding to a required lift coefficient of 1.24 and a required moment coefficient of 0). The flow solver was initialized with an angle of attack of 5 deg and with no elevator deflection. Although a much closer estimate of the values of the trim variables was available from linear trim analysis, the flow solver was initialized with these values to demonstrate the robustness of the trim algorithm with respect to initial trim variables. Figure 10 shows the CFD error decay of the trim-run cases compared to that of a rigid configuration (started with the final values of trim variables $\alpha = 9.8$ deg and $\delta = -12.9$ deg). It is seen that the CFD error decay plots are parallel, with an increase of the error following the first trim correction. This increase is proportional to the modification introduced to the trim variables and is smaller when starting with a closer estimate of the trim variables.

Figure 11 shows the history of convergence of the lift and moment coefficients, indicating the approach to their trimmed values. It is seen that only five trim updates are required for convergence of the aerodynamic coefficients. Figure 12 shows the values of the angle of attack and elevator deflection angle after each trim correction. The analysis also provides the aerodynamic load distribution acting on the maneuvering aircraft, which can be used for structural load analysis and structural design.

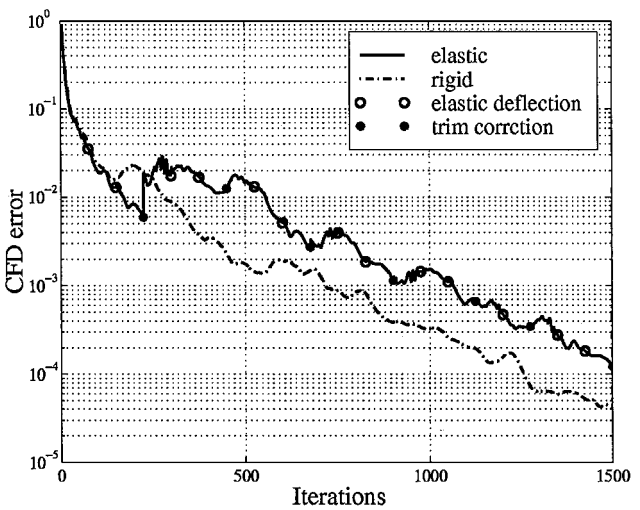

Fig. 10 Residual decay history.

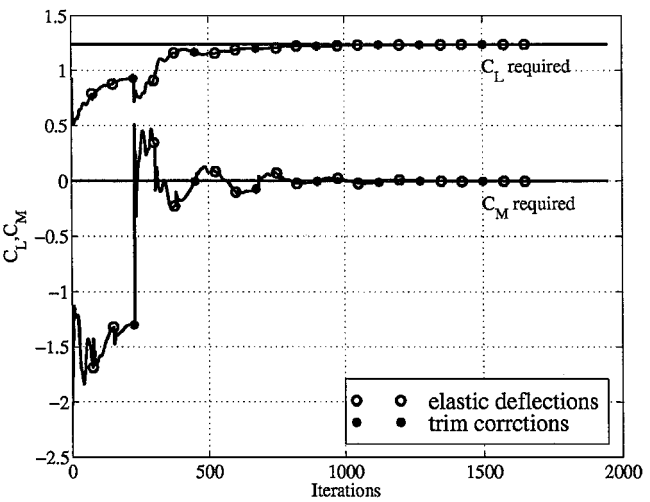

Fig. 11 C_L and C_M convergence history.

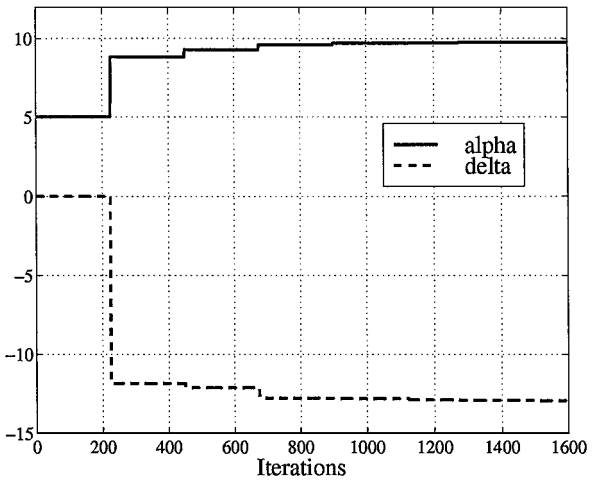

Fig. 12 Alpha and delta convergence history.

Conclusions

The paper presented an efficient integrated aerodynamic–structural scheme for evaluating maneuver loads on a flexible aircraft, using nonlinear aerodynamic theory. The maneuver scheme is based on a conventional Navier–Stokes/Euler code that was originally developed for fixed-shape configurations. The CFD code was supplemented with a modal structural model to account for aircraft elasticity and with a maneuver attainment algorithm. The use of normal modes for the representation of the structure was accurate and provided a simple interface between the CFD and the structure that requires a minimum of structural information to be imported to the CFD routine. The use of the modal representation also facilitated a simple CFD grid update following each deformation update. The maneuver-load scheme, which is based on elastic deflections and trim corrections that are applied during steady-state flowfield convergence, showed very good convergence properties, with a number of iterations required for convergence almost identical to that of the fixed-shape configuration. Also, the extra CPU time required for the elastic deformations and trim corrections was shown to be small compared to the total run time. The direct calculation of loads for a specific user-defined maneuver facilitates the inclusion of the trim proposed scheme in automatic structural design procedures for flight vehicles and in procedures for combined aerodynamic–structural design optimization.

References

[1]Albano, E., and Rodden, W. P., "A Doublet-Lattice Method for Calculating Lift Distributions on Oscillating Surfaces in Subsonic Flows," *AIAA Journal*, Vol. 7, No. 2, 1969, pp. 279–285.

[2]Rodden, W. P., and Johnson, E. H., "MSC/NASTRAN Version 68 Aeroelastic Analysis User's Guide," Macneal–Schwendler Corp., CA, 1994.

[3]Neill, D. J., Johnson, E. H., and Canfield, R. A., "ASTROS: A Multidisciplinary Automated Structural Design Tool," *Journal of Aircraft*, Vol. 27, No. 12, 1990, pp. 1021–1027.

[4]Whitlow, W., Jr., and Bennett, R. M., "Application of a Transonic Potential Flow Code to the Static Aeroelastic Analysis of Three-Dimensional Wings," *Proceedings of the 23rd Structures, Structural Dynamics, and Materials Conference*, Vol. 2, AIAA, Washington, DC, pp. 267–276.

[5]Agrell, N., and Hedman, S. G., "Calculations of Transonic Steady State Aeroelastic Effects for Canard Airplane," *Proceedings of the 13th Congress of the International Council of the Aeronautical Sciences, AIAA Aircraft System and Technology Conference*, AIAA, Washington, DC, pp. 59–66.

[6]Pittman, J. L., and Giles, G. L., "Combined Nonlinear Aerodynamic and Structural Method for the Aeroelastic Design of a Three-Dimensional Wing in Supersonic Flow," *Proceedings of the Applied Aerodynamics Conference*, AIAA, Washington, DC, pp. 36–44.

[7]Tatum, K. E., and Giles, G. L., "Integrating Nonlinear Aerodynamic and Structural Analysis for a Complete Fighter Configuration," *Journal of Aircraft*, Vol. 25, No. 12, 1988, pp. 1150–1156; also AIAA Paper 87-2863, 1987.

[8]Vinh, L., Edwards, J. W., Seidel, D. A., and Batina, J. T., "Transonic Stability and Control of Aircraft Using CFD Methods," *Proceedings of the AIAA Atmospheric Flight Mechanics Conference*, AIAA, Washington, DC, 1988, pp. 394–404.

[9]Batina, J. T., Seidel, D. A., Bland, S. R., and Bennet, R.M., "Unsteady Transonic Flow Calculations for Realistic Aircraft Configurations," *Proceedings of the 28th Structures, Structural Dynamics, and Materials Conference*, AIAA, Washington, DC, 1987, pp. 21–28.

[10]Schuster, D. M., Vadyak, J., and Atta, E., "Static Aeroelastic Analysis of Fighter Aircraft Using a Three-Dimensional Navier–Stokes Algorithm," *Journal of Aircraft*, Vol. 27, No. 5, 1990, pp. 820–825.

[11]Schuster, D. M., "Application of a Navier–Stokes Aeroelastic Method to Improve Fighter Wing Performance at Maneuver Flight Conditions," *Journal of Aircraft*, Vol. 32, No. 1, 1995, pp. 77–83.

[12]Guruswamy, G. P., "Coupled Finite-Difference/Finite-Element Approach for Wing-Body Aeroelasticity," *Proceedings of the 4th Symposium on Multidisciplinary Analysis and Optimization*, AIAA, Washington, DC, 1992, pp. 1–12.

[13]Obayashi, S., and Guruswamy, G. P., "Convergence Acceleration of Navier–Stokes Solver for Efficient Static Aeroelastic Computations," *AIAA Journal*, Vol. 33, No. 6, 1996, pp. 1134–1141.

[14]Sheena, Z., and Karpel, M., "Static Aeroelastic Analysis Using Aircraft Vibration Modes," *Proceedings of the 2nd International Symposium on Aeroelasticity and Structural Dynamics*, DGLR Aachen Germany, 1985, pp. 229–232.

[15]Karpel, M., and Sheena, Z., "Structural Optimization for Aeroelastic Control Effectiveness," *Journal of Aircraft*, Vol. 26, No. 8, 1989, pp. 493–495.

[16]Karpel, M., Yaniv, S., and Livshits, D. S., "Integrated Solution for Computational Static Aeroelastic Problems," *Journal of Spacecraft and Rockets*, Vol. 35, No. 5, 1998, pp. 612–618; also AIAA Paper 96-4012, 1996.

[17]Yaniv, S., "Navier–Stokes Calculations for Rotating Configurations: Implementation for Rockets," *Journal of Spacecraft*, Vol. 33, No. 5, 1996, pp. 756–758.

[18]Harder, R. L., and Desmarais, R. N., "Interpolation Using Surface Splines," *Journal of Aircraft*, Vol. 9, No. 2, 1972, pp. 189–191.